Available online at www.sciencedirect.com
SCIENCE DIRECT®
Thin Solid Films 440 (2003) 78–86
thin solid films
www.elsevier.com/locate/tsf

The process window for diamond deposition from the vapor phase with sulfur in the C–H–O feed gas mixtures

Gopinath Bhimarasetti, Mahendra K. Sunkara*

Department of Chemical Engineering, University of Louisville, Louisville, KY 40292, USA

Received 21 March 2003; received in revised form 17 May 2003; accepted 19 May 2003

Abstract

Theoretical predictions using a modified radical species ternary diagram for C–H–O system indicate that addition of sulfur expands the C–H–O gas phase compositional window for diamond deposition. Sulfur addition to no-growth domain increases the carbon super-saturation by binding the oxygen and the addition of sulfur to the non-diamond domain reduces the heavy carbon super-saturation by decreasing C_nH_m species concentration in the gas phase. The overall effect of sulfur addition to gas phase mixtures is characterized as that of oxygen addition to the C–H system, i.e. expansion of the compositional window over which diamond can be deposited from the gas phase. In addition, the increasing sulfur concentration to diamond domain feed gases beyond 2000 ppm did not affect the steady state gas phase composition but the quality of diamond was reduced.

Keywords: Diamond; Reaction kinetics; Sulfur; Chemical vapor deposition

1. Introduction

Diamond deposition from the vapor phase in the presence of dopants has gained particular importance with reports on sulfur doping [1–3] and co-doping [4] involving sulfur. However, currently there is no empirical diagram or a method to predict diamond deposition from the vapor phase containing dopant species such as boron and sulfur. There have been attempts to obtain useful criterion for predicting diamond deposition domain using radical species composition [5]. Eaton and Sunkara [6] proposed a ternary plot based on C–H–O radical species to predict the diamond deposition and demonstrated the use of such diagram for predicting the deposition in micro-trenches [7]. However, the question of predictability of diamond deposition domain in the presence of fourth element such as sulfur in the gas phase has not been addressed. Dandy [8] reported equilibrium calculations to explain gas phase chemistry effects on the incorporation of nitrogen and sulfur during diamond deposition. Sternschulte et al. [9] reported decrease in growth rates with sulfur addition and reported a decrease in experimentally measured concentration of CH_3 species with increasing H_2S in the gas phase. Petherbridge et al. [10] reported gas phase kinetics calculations for CH_4/CO_2 system with H_2S addition to explain the decrease in growth rates and identified increase in CS, CS_2, SO and SO_2 with increasing H_2S in the feed gases. The calculations were, however, performed at 2000 K, far away from the actual diamond growing conditions. We note that the diamond deposition is kinetics limited and that the radical species composition at gas–surface interface is directly relevant. We, therefore, performed our calculations at 1150 K, close to the actual diamond growing conditions.

In a manner similar to the effect of residence time, temperature and pressure on the deposition domain [6], we postulate that the changes in C–H–O radical species composition in the presence of dopant species could be used to predict the deposition domain. In this regard, we obtained a modified C–H–O radical species diagram, including the feed gas compositions from C–H line. Secondly, we obtained the changes in the C–H–O radical species compositions with the addition of sulfur and predicted the diamond deposition. The computation-

*Corresponding author. Tel.: +1-502-852-1558; fax: +1-502-852-6355.
E-mail address: mahendra@louisville.edu (M.K. Sunkara).

0040-6090/03/$ - see front matter © 2003 Elsevier B.V. All rights reserved.
doi:10.1016/S0040-6090(03)00837-X

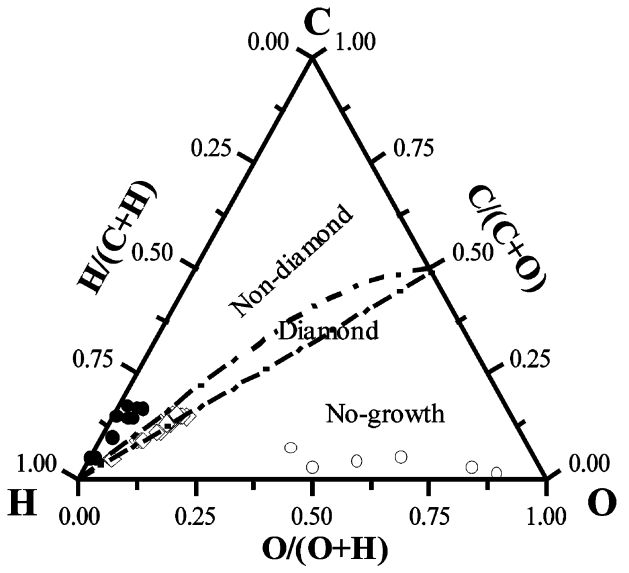

Fig. 1. The C–H–O feed gas compositional ternary plot by Bachmann et al. [14]. (●) chosen data points from non-diamond domain, (□) data points from diamond domain and (○) data points from no-growth domain.

al results are compared with the experimental work published previously [9,10] and also with the experimental observations from this work.

2. Computations

Steady state gas phase compositions were computed using detailed reaction sets compiled for C–H–O and C–H–O–S systems. The steady state computations were performed using CHEMKIN III Aurora software package (Reaction Design Inc., CA) for gas–substrate interface as a zero dimensional model. The compositions of the gas phase species were then analyzed by dividing them into participating and non-participating species as described in Ref. [6]. In addition, to the non-participating species considered in Ref. [6] (CH_4, O_2, H_2, H_2O, CO, CO_2) sulfur containing species were also considered as non-participating in this work. The atom fractions of C, H and O of the participating species were plotted on a C–H–O ternary diagram.

3. Experimental details

A hot-filament reactor with independent substrate heating was used to conduct diamond deposition experiments with CH_4, H_2, O_2 and H_2S as feed gases. A 0.5 mm tungsten wire was wound into a spring and used as the filament, while maintaining a distance of 8–10 mm from the substrate. The experiments were performed at 40 torr pressure and substrate temperature of approximately 720 °C, measured using a backside thermocouple.

4. Results and discussion

4.1. Modified C–H–O radical species diagram

First, the C–H–O radical species diagram was reconstructed using a more detailed reaction set for gas phase chemistry than the one used in Ref. [6] while retaining the same set of surface reactions. The gas phase chemistry was compiled from different sources [11,12]. Several feed gas points, as shown in Fig. 1, in the three deposition domains of the lens-shaped, Bachmann feed gas diagram [13,14] were chosen. In the ternary diagram proposed in Ref. [6], the domain on the C–H line was not considered. Here, we also included several feed gas compositions on the C–H line for analysis. The steady state gas phase species compositions corresponding to the chosen feed gases are calculated and the overall C, H and O atom fractions from the 'participating' species are plotted on the C–H–O ternary plot. The resulting ternary diagram is shown in Fig. 2. According to the ternary diagram based on feed gases, the cut off between diamond and non-diamond regions is around $H/(C+H)$ of 0.98. When this cut off is represented on the radical species based ternary plot, the boundary between the diamond and non-diamond is at about $H/(C+H)=0.57$, as shown in Fig. 2.

As shown in Fig. 2, the composition of 'participating' C–H–O radical species could distinguish diamond deposition, no-deposition and non-diamond deposition. The resulting domain for diamond deposition is trapezoidal with the inclusion of domain on the C–H line. The distinction between no-growth and diamond domain in the modified plot is very fine, with the no-growth

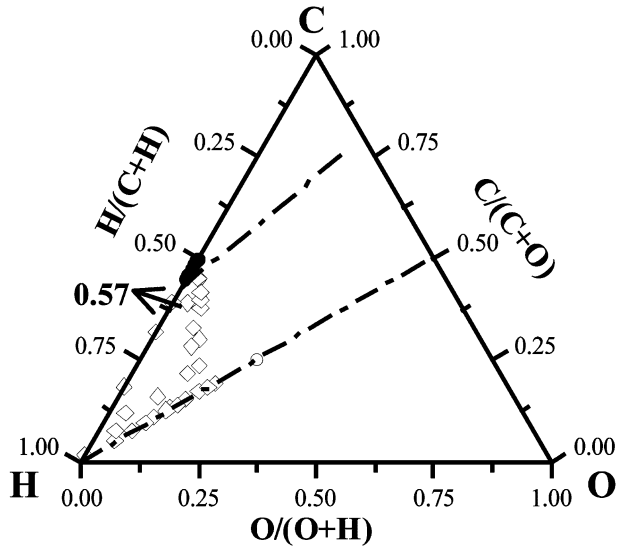

Fig. 2. Modified C–H–O ternary diagram constructed based on the overall radical species compositions calculated for the points from Fig. 1.

domain points just below the CO tie line. All the points in the diamond domain are above this line. This behavior at the CO tie line is in agreement with the equilibrium calculations of Prijaya et al. [15].

4.2. Diamond deposition domain with C–H–O–S gas phase

We compiled a C–H–O–S chemistry set to analyze the changes in C–H–O species concentration with addition of sulfur in the gas phase. The compiled set consisted of 28 C–H–O species and 13 C–H–O–S species. The overall reaction set consisted of 143 C–H–O and 73 C–H–O–S gas phase reactions (Table 1) along with 12 surface reactions (Table 2). No surface reactions involving sulfur were used due to lack of kinetics data. The sulfur gas phase chemistry set was primarily compiled from Ref. [11].

The calculated steady state compositions of C–H–O–S species were analyzed as following: A data point from the non-diamond domain of the C–H line from the Bachmann diagram was chosen. For CH_4–H_2 feed gases, the distinction between diamond and non-diamond domains according to Bachmann diagram is at 4% CH_4. Calculations were performed on the data point corresponding to 5% CH_4 in H_2 with increasing amounts of H_2S. The position of the resulting C–H radical species composition moved to the diamond domain with addition of a few ppm of H_2S. This implies that addition of H_2S to feed gas compositions from non-diamond domain affected the radical species concentrations in a way that the resulting composition fell within the diamond domain. The heavy carbon super-saturation was reduced with the addition of sulfur by decreasing the C_nH_m radicals' concentrations as shown in Fig. 3.

Similar trends were observed for other points chosen from the non-diamond domain of the feed gas diagram. The concentration of CH_3 and C_2H_2 species decreased by 2–4 orders of magnitude, respectively, with the addition of few hundred ppm of H_2S in the feed gas. This is an indication that the heavy super saturation, typical of non-diamond domain, was reduced, thus causing a transition from non-diamond to diamond domain. The amount of sulfur needed in the non-diamond domain feed gases to cause a transition from non-diamond domain to diamond domain decreases towards the 'C' vertex on the C–H–O ternary diagram. The tolerance of the system to sulfur is higher when it is closer to the non-diamond and diamond domain boundary, but decreases as we move towards the 'C' vertex. Calculations performed for non-diamond domain feed gases from the C–H–O domain indicate that the addition of sulfur moves the resulting composition into diamond domain. The dominant sulfur containing species are SO_2, S_2 and H_2S, which increase with increasing H_2S in the feed gases. The decrease in CH_3 and C_2H_2 species radicals could be explained by the increase in CH_4 concentration by two orders of magnitude. In combustion literature, sulfur has been found to be catalytic inhibitor [16–18]. Similar behavior is observed with C–H–O system at diamond growing conditions, i.e. addition of sulfur enhanced recombination reactions leading to more stable molecules, CH_4 and H_2 in the gas phase. No significant CS/CS_2 species were found from our calculations at 1150 K. The prior computations by Petherbridge et al. [10] at 2000 K predicted significant concentrations of CS and CS_2 species. At these temperatures, the effect of sulfur is somewhat more direct, i.e. sulfur binds to carbon in the form of CS and CS_2 species. In fact, the negligible concentrations of CS/CS_2 found near diamond growing conditions could explain why the incorporation of sulfur is considered difficult.

Similar results were obtained with feed gas data points from other domains, i.e. diamond deposition and no-deposition. In all the cases, the C_nH_m radicals decreased with addition of sulfur. The addition of sulfur did not change the overall radical species (or 'participating species') composition significantly for feed gas compositions from diamond domain. The net effect is that the overall composition for the participating species stayed within diamond domain even with addition of sulfur in excess of 10000 ppm. In the no-growth domain, the decrease in C_nH_m species is compensated by a greater decrease in the oxygenated species, such as O and OH, as shown in Fig. 4. The increase in mole fraction of O_2 shown in Fig. 4 can be explained by the decrease in mole fractions of O, OH and CO. Thus, the carbon super saturation was relatively increased, causing the resulting overall composition to fall in to the diamond domain. The dominant sulfur species were SO_2, SO_3, SO, H_2S and S_2.

The behavior of the gas phase on the C–H–O radical diagram with addition of sulfur to no-growth domain and non-diamond domain is summarized in Fig. 5. In both the cases, sulfur seems to have adjusted the super saturation such that the resulting overall C–H–O radical species composition falls into the diamond deposition domain. Experiments were conducted to confirm these predictions on the effect of sulfur on diamond deposition for feed gas composition from the non-diamond deposition and no-growth domains. The experiments using feed gases with 10% CH_4 in H_2 resulted in ballas type diamond crystals as shown in Fig. 7. This illustrates that super-saturation could be reduced by introducing sulfur into the gas phase. However, at higher CH_4 concentrations no diamond could be nucleated and grown as predicted by calculations. Non-diamond carbon deposit was formed at these higher CH_4 concentrations.

Another set of experiments were done at feed gas composition of 1% CH_4 and 1% O_2 in H_2. This corresponds to $C/(C+O)$ value of $1/(1+2)=0.33$.

Table 1
List of all the elementary gas phase reactions used in the model. Rate constant $k=A\times(T)^b \exp(-E/RT)$. A is the pre-exponential factor, b is the temperature exponent and E is the activation energy

No	Gas phase reactions considered	A (cm-mol-s)	b	E (cal-mol)	No	Gas phase reactions considered	A (cm-mol-s)	b	E (cal-mol)
1	$H+H+M=H_2+M$	1.00×10^{18}	−1	0	109	$CH+H_2O=CH_2O+H$	1.17×10^{15}	−0.8	0
2	$H+H+H_2=2H_2$	9.20×10^{16}	−0.6	0	110	$CH+CH_2O=CH_2CO+H$	9.46×10^{13}	0	−515
3	$H+H+H_2O=H_2+H_2O$	6.00×10^{19}	−1.2	0	111	$CH+CH_2=C_2H_2+H$	4.00×10^{13}	0	0
4	$H+H+CO_2=H_2+CO_2$	5.49×10^{20}	−2	0	112	$CH+CH_3=C_2H_3+H$	3.00×10^{13}	0	0
5	$O+OH=O_2+H$	4.00×10^{14}	−0.5	0	113	$CH+CH_4=C_2H_4+H$	6.00×10^{13}	0	0
6	$O+H_2=OH+H$	5.06×10^{4}	2.7	6290	114	$C_2H_3+CH=CH_2+C_2H_2$	5.00×10^{13}	0	0
7	$2OH=O+H_2O$	1.50×10^{9}	1.1	99	115	$HCCO+CH=C_2H_2+CO$	5.00×10^{13}	0	0
8	$2O+M=O_2+M$	1.20×10^{17}	−1	0	116	$CH+CO+M=HCCO+M$	5.00×10^{13}	0	0
9	$H_2+O_2=2OH$	1.70×10^{13}	0	47780	117	$OH+C=H+CO$	5.00×10^{13}	0	0
10	$OH+H_2=H_2O+H$	1.17×10^{9}	1.3	3626	118	$C+O_2=O+CO$	5.80×10^{13}	0	575
11	$CH_4+O=CH_3+OH$	1.02×10^{9}	1.5	8604	119	$C+CH_2=H+C_2H$	5.00×10^{13}	0	0
12	$CH_4+H=CH_3+H_2$	1.32×10^{4}	3	8040	120	$C+CH_3=H+C_2H_2$	5.00×10^{13}	0	0
13	$CH_4+OH=CH_3+H_2O$	1.60×10^{6}	2.1	2460	121	$HCO+M=CO+H+M$	2.50×10^{14}	0	16802
14	$CH_4+O_2=CH_3+HO_2$	7.90×10^{13}	0	56000	122	$HCO+H=CO+H_2$	1.19×10^{13}	0.2	0
15	$CH_4+HO_2=CH_3+H_2O_2$	1.13×10^{13}	0	24641	123	$HCO+O=CO+OH$	3.00×10^{13}	0	0
16	$CH_3+H=CH_2+H_2$	9.00×10^{13}	0	15100	124	$HCO+O=CO_2+H$	3.00×10^{13}	0	0
17	$CH_3+O=CH_2O+H$	8.00×10^{13}	0	0	125	$HCO+OH=CO+H_2O$	1.00×10^{14}	0	0
18	$CH_3+OH=CH_2+H_2O$	7.50×10^{6}	2	5000	126	$HCO+O_2=CO+HO_2$	7.60×10^{12}	0	400
19	$CH_3+OH=CH_3O+H$	5.74×10^{12}	−0.2	13931	127	$CH_3+HCO=CH_4+CO$	1.20×10^{14}	0	0
20	$CH_3+O_2=CH_3O+O$	2.05×10^{18}	−1.6	29229	128	$O+CO+M=CO_2+M$	6.17×10^{14}	0	3000
21	$CH_3+O_2=CH_2O+OH$	3.59×10^{09}	−0.1	10150	129	$CO+OH=CO_2+H$	1.51×10^{7}	1.3	−758
22	$CH_3+HO_2=CH_3O+OH$	2.00×10^{13}	0	0	130	$O_2+CO=O+CO_2$	2.50×10^{12}	0	47800
23	$CH_3+CH_3=C_2H_4+H_2$	1.00×10^{16}	0	2005	131	$CO+HO_2=CO_2+OH$	5.80×10^{13}	0	22934
24	$CH_2+OH=CH_2O+H$	2.50×10^{13}	0	0	132	$C_2H_2+H=C_2H+H_2$	6.02×10^{13}	0	22243
25	$CH_2+O=CO+2H$	5.00×10^{13}	0	0	133	$C_2H+O=CH+CO$	1.81×10^{13}	0	0
26	$CH_2+CO_2=CH_2O+CO$	1.10×10^{11}	0	1000	134	$H_2O_2+OH=H_2O+HO_2$	1.75×10^{12}	0	320
27	$CH_2+O=CO+H_2$	3.00×10^{13}	0	0	135	$O+HO_2=O_2+OH$	1.75×10^{13}	0	−400
28	$CH_2+O_2=CO_2+2H$	1.60×10^{12}	0	1000	136	$H+HO_2=2OH$	1.69×10^{14}	0	874
29	$CH_2+O_2=CO+H_2O$	1.90×10^{10}	0	−1000	137	$H+HO_2=H_2+O_2$	6.62×10^{13}	0	2130
30	$CH_2+O_2=CO+OH+H$	8.60×10^{10}	0	−500	138	$OH+HO_2=H_2O+O_2$	1.45×10^{16}	−1	0
31	$CH_2+O_2=HCO+OH$	4.30×10^{10}	0	−500	139	$H_2O_2+O_2=2HO_2$	5.42×10^{13}	0	39740
32	$CH_2+O_2=CH_2O+O$	2.00×10^{14}	0	10000	140	$HO_2+H_2=H_2O_2+H$	3.01×10^{13}	0	26030
33	$CH_2+O_2=CO_2+H_2$	6.90×10^{11}	0	500	141	$OH+M=O+H+M$	2.42×10^{15}	0	99360
34	$CH_2+CH_3=C_2H_4+H$	3.00×10^{13}	0	0	142	$H_2O_2+M=2OH+M$	1.29×10^{33}	−4.9	53250
35	$2CH_2=C_2H_2+H_2$	4.00×10^{13}	0	0	143	$H_2O+M=H+OH+M$	3.49×10^{15}	0	105120
36	$CH_2+HO_2=CH_2O+OH$	3.01×10^{13}	0	0	144	$HO_2+M=H+O_2+M$	1.21×10^{19}	−1.2	48410
37	$CH_2+H_2O_2=CH_3O+OH$	3.01×10^{13}	0	0	145	$H+H_2O_2=H_2O+OH$	2.41×10^{13}	0	3970
38	$CH_2+CH_2O=CH_3+HCO$	1.20×10^{12}	0	0	146	$O_2+C_2H_5=C_2H_4+HO_2$	8.43×10^{11}	0	3880
39	$CH_2+HCO=CH_3+CO$	1.81×10^{13}	0	0	147	$H_2O+C_2H_5=C_2H_6+OH$	3.39×10^{6}	1.4	20270
40	$CH_2+H=CH+H_2$	1.00×10^{18}	−1.6	0	148	$H_2O_2+C_2H_5=C_2H_6+HO_2$	8.73×10^{9}	0	970
41	$CH_2+OH=CH+H_2O$	1.13×10^{07}	2	3000	149	$OH+C_2H_5=C_2H_4+H_2O$	2.41×10^{13}	0	0
42	$CH+O_2=HCO+O$	3.30×10^{13}	0	0	150	$OH+C_2H_5=C_2H_6+O$	9.90×10^{17}	8.8	500
43	$CH+O=CO+H$	5.70×10^{13}	0	0	151	$HO_2+C_2H_5=C_2H_6+O_2$	3.01×10^{11}	0	0
44	$H+CH=C+H_2$	1.10×10^{14}	0	0	152	$HCO+C_2H_5=C_2H_6+CO$	1.21×10^{14}	0	0
45	$CH+OH=HCO+H$	3.00×10^{13}	0	0	153	$C_2H_5+O=CH_2O+CH_3$	1.61×10^{13}	0	0
46	$CH+CO_2=HCO+CO$	3.40×10^{12}	0	690	154	$CH_2O+C_2H_5=C_2H_6+HCO$	5.49×10^{03}	2.8	5860
47	$CH_2CO+CH_3=CO+C_2H_5$	5.00×10^{12}	0	0	155	$CH_2CO+OH=CO+CH_2OH$	6.12×10^{12}	0	0
48	$C_2H_6+CH_2=CH_3+C_2H_5$	6.46×10^{12}	0	7910	156	$CH_2CO=H+HCCO$	4.00×10^{8}	0	0
49	$C_2H_6+C_2H_2=C_2H_3+C_2H_5$	9.64×10^{11}	0	4570	157	$CH_2CO=CO+CH_2$	3.60×10^{15}	0	59220
50	$C_2H_6+M=C_2H_4+H_2+M$	2.29×10^{17}	0	67570	158	$H_2S+O=H+HSO$	3.01×10^{13}	0	7650
51	$H+C_2H_5=C_2H_6$	4.50×10^{13}	0	0	159	$H_2S+O=OH+SH$	1.21×10^{14}	0	7650
52	$CH_3+CH_3+M=C_2H_6+M$	1.26×10^{41}	−7	2760	160	$H_2S+H=H_2+SH$	2.20×10^{17}	1.9	900
53	$C_2H_5+C_2H_5=C_2H_6+C_2H_4$	1.45×10^{12}	0	0	161	$H_2S+M=H+SH+M$	1.76×10^{16}	0	66170
54	$H_2+C_2H_5=C_2H_6+H$	3.07	3.6	8450	162	$H_2S+M=H_2+S+M$	1.90×10^{14}	0	65380
55	$C_2H_2+C_2H_5=C_2H_6+C_2H$	2.71×10^{11}	0	23450	163	$OH+H_2S=H_2O+SH$	3.67×10^{12}	0	160
56	$C_2H_4+C_2H_5=C_2H_6+C_2H_3$	6.32×10^{2}	3.1	18000	164	$CH_3+H_2S=CH_4+SH$	1.26×10^{11}	0	2310
57	$CH_4+CH_3=C_2H_6+H$	1.00×10^{9}	1	44910	165	$SH+O=H+SO$	7.83×10^{13}	0	0
58	$CH_4+C_2H_5=C_2H_6+CH_3$	8.60×10^{-2}	4.1	12560	166	$SH+O=OH+S$	2.29×10^{11}	0.7	1900
59	$CH_3+C_2H_5=CH_4+C_2H_4$	1.95×10^{13}	−0.5	0	167	$SH+SH=S+H_2S$	3.98×10^{12}	0	0
60	$C_2H+C_2H_5=C_2H_4+C_2H_2$	1.81×10^{12}	0	0	168	$SH+SH=H_2+S_2$	3.01×10^{10}	0	0
61	$C_2H_5+CH_2=C_2H_4+CH_3$	1.81×10^{13}	0	0	169	$H+SH=H_2+S$	1.02×10^{13}	0	0

Table 1 *(Continued)*

No	Gas phase reactions considered	*A* (cm-mol-s)	*b*	*E* (cal-mol)	No	Gas phase reactions considered	*A* (cm-mol-s)	*b*	*E* (cal-mol)
62	$CH_3+CH_3=H+C_2H_5$	2.40×10^{13}	0	12880	170	$O_2+SH=O+HSO$	1.87×10^{13}	0	17920
63	$C_2H_4+H+M=C_2H_5+M$	2.79×10^{18}	0	760	171	$O_2+SH=OH+SO$	2.41×10^{5}	0	0
64	$C_2H_4+H_2=H+C_2H_5$	1.02×10^{13}	0	68160	172	$S+SH=H+S_2$	3.00×10^{12}	0	0
65	$C_2H_4+C_2H_4=C_2H_3+C_2H_5$	4.82×10^{14}	0	71540	173	$CO+SH=COS+H$	2.50×10^{10}	0	15220
66	$CH_4+CH_3=H_2+C_2H_5$	1.00×10^{13}	0	23050	174	$HSO=H+SO$	8.43×10^{15}	0	58620
67	$CH_3+H+M=CH_4+M$	8.00×10^{26}	−3	0	175	$O_2+HSO=OH+SO_2$	1.02×10^{09}	0	0
68	$CH_4+CH_2=CH_3+CH_3$	1.00×10^{13}	0	0	176	$HSO_2=HOSO$	1.62×10^{9}	1.3	25950
69	$CH_3+M=CH_2+H+M$	1.00×10^{16}	0	90600	177	$H+HSO_2=H_2+SO_2$	3.01×10^{12}	0	0
70	$C_2H_4+M=C_2H_2+H_2+M$	2.60×10^{17}	0	79400	178	$O_2+HSO_2=HO_2+SO_2$	1.81×10^{11}	0	0
71	$C_2H_4+M=C_2H_3+H+M$	2.60×10^{17}	0	96600	179	$OH+HSO_2=SO_2+H_2O$	4.82×10^{12}	0	0
72	$C_2H_4+H=C_2H_3+H_2$	1.10×10^{14}	0	8500	180	$HSO_2=O+HSO$	1.44×10^{17}	−1.1	28380
73	$C_2H_4+CH_3=CH_4+C_2H_3$	4.20×10^{11}	0	11200	181	$M+HOSO=M+HSO_2$	1.92×10^{21}	−5.6	55420
74	$C_2H_3+H=C_2H_2+H_2$	2.00×10^{13}	0	0	182	$M+HSO_2=O+HSO$	2.77×10^{20}	−5.9	30960
75	$C_2H_3+M=C_2H_2+H+M$	3.00×10^{15}	0	32000	183	$M+HSO_2=O_2+SH$	1.64×10^{16}	−2.8	7450
76	$C_2H_3+CH_3=C_2H_2+CH_4$	7.90×10^{11}	0	0	184	$SO+O+M=SO_2+M$	1.20×10^{22}	−1.8	0
77	$C_2H_2+M=C_2H+H+M$	4.00×10^{16}	0	107000	185	$SO+SO=SO_2+S$	1.21×10^{11}	0	0
78	$C_2H_2+CH_3=C_2H_3+CH_2$	3.10×10^{14}	0	69888	186	$SO+M=S+O+M$	3.98×10^{14}	0	107000
79	$C_2H_2+C_2H_2=C_2H_3+C_2H$	3.10×10^{14}	0	91208	187	$SO_3+SO=SO_2+SO_2$	1.20×10^{9}	0	0
80	$CH_3CO=C_2H_2+OH$	2.20×10^{12}	0	30010	188	$OH+SO=SO_2+H$	5.18×10^{13}	0	0
81	$CH_3CO+O_2=CH_2O+CO+OH$	1.81×10^{10}	0	0	189	$OH+SO=HOSO$	2.69×10^{13}	0.5	−400
82	$CH_3CO=CH_2CO+H$	1.58×10^{13}	0	34970	190	$OH+M+SO=M+HOSO$	1.44×10^{13}	−3.5	970
83	$CH_3CO+CH_2=CH_2CO+CH_3$	1.81×10^{13}	0	0	191	$SO_2+O=O_2+SO$	5.00×10^{12}	0	19470
84	$CH_3CO+O=CH_2CO+OH$	3.86×10^{13}	0	0	192	$SO_2+H=HSO_2$	1.39×10^{13}	0.6	3620
85	$CH_3CO+O=CO_2+CH_3$	9.64×10^{12}	0	0	193	$SO_2+H=HOSO$	2.21×10^{12}	1	8580
86	$CH_3CO+H=CH_3+HCO$	1.30×10^{13}	0	0	194	$HO_2+SO_2=OH+SO_3$	1.21×10^{7}	0	0
87	$CH_3CO+H=CH_2CO+H_2$	7.00×10^{12}	0	0	195	$M+SO_2+H=M+HSO_2$	1.09×10^{20}	−3.7	4790
88	$CH_3CO+O_2=CO_2+CH_3O$	4.40×10^{10}	0	1080	196	$M+SO_2+H=M+HOSO$	3.42×10^{20}	−4.4	10810
89	$CH_3CO+OH=CH_2CO+H_2O$	1.21×10^{13}	0	0	197	$SO_3+O=SO_2+O_2$	6.50×10^{14}	0	10810
90	$CH_3CO=CO+CH_3$	8.74×10^{42}	−8.6	22460	198	$SO_3+M=SO_2+O+M$	3.16×10^{15}	0	63390
91	$CH_2CO+CH_2=CH_3+HCCO$	6.03×10^{06}	0	0	199	$CS+O=CO+S$	3.01×10^{13}	0	0
92	$CH_2CO+CH_2=C_2H_4+CO$	1.26×10^{14}	0	0	200	$CS+O_2=CO+SO$	8.45×10^{4}	0	0
93	$CH_2CO+H=CO+CH_3$	3.73×10^{10}	0	0	201	$CS+O_2=COS+O$	1.58×10^{08}	0	3700
94	$CH_2CO+OH=H_2O+HCCO$	1.02×10^{11}	0	0	202	$COS+C=CO+CS$	6.08×10^{13}	0	0
95	$CS_2+O=CS+SO$	1.21×10^{13}	0	1030	203	$SO=S+O$	3.98×10^{14}	0	107000
96	$CS_2+O=CO+S_2$	6.50×10^{10}	0	0	204	$H_2S=H_2+S$	4.00×10^{14}	0	65580
97	$CS_2+O=COS+S$	2.20×10^{12}	0	1390	205	$COS+O=CO_2+S$	5.00×10^{13}	0	19990
98	$CS_2+O_2=CS+SO_2$	1.00×10^{12}	0	31990	206	$COS=CO+S$	2.45×10^{14}	0	61400
99	$CS_2+S=CS+S_2$	1.70×10^{14}	0	11760	207	$CS_2=CS+S$	2.51×10^{14}	0	74320
100	$CS_2+OH=COS+SH$	1.21×10^{9}	0	0	208	$O_2+SH=HSO_2$	2.07×10^{13}	0.3	0
101	$CS_2+M=CS+S$	2.51×10^{14}	0	74320	209	$HO_2+SH=OH+HSO$	6.03×10^{12}	0	0
102	$S+O_2=SO+O$	1.51×10^{13}	0	3660	210	$H_2S=H+SH$	1.76×10^{16}	0	66170
103	$S+S+M=S_2+M$	4.30×10^{18}	0	0	211	$COS+OH=CO_2+SH$	2.41×10^{10}	0	0
104	$OH+S=H+SO$	3.97×10^{13}	0	0	212	$HO_2+H_2S=H_2O+HSO$	3.01×10^{12}	0	0
105	$C_2H_6+S=SH+C_2H_5$	1.23×10^{14}	0	14750	213	$SO+O=SO_2$	3.20×10^{13}	0	0
106	$CH_4+S=CH_3+SH$	2.04×10^{14}	0	19870	214	$O_2+SO=SO_3$	4.89×10^{11}	0	5730
107	$S_2=S+S$	4.79×10^{13}	0	76900	215	$COS+O=CO+SO$	1.26×10^{13}	0	4370
108	$O+S_2=S+SO$	1.00×10^{13}	0	0	216	$SO_2+O=SO_3$	5.83×10^{5}	3.6	0

This point, according to the Bachmann diagram lies in no-growth region. The position of this data point moves into diamond domain with addition of sulfur as shown in Fig. 5. The deposition experiments with 1% CH_4 and 1% O_2 were done using 1500 ppm of H_2S. Diamond crystals nucleated and grew with a growth rate of 83 nm/h. The SEM micrographs are shown in Fig. 7. Experiments were also conducted at higher O_2 concentrations with 1% CH_4 in H_2. In these experiments, the tungsten filament sputtered onto the substrate due to the presence of higher amount of oxygen. Energy dispersive X-ray spectroscopy on the deposited films indicated the presence of both Tungsten and carbon.

4.3. The effect of sulfur on growth rates

It is observed that growth rates decrease with addition of sulfur to feed gases from the diamond domain. Sternschulte [9] and Petherbridge [10] have indicated that the drop in growth rates is due to the drop in CH_3 radicals from their in situ measurements of the gas phase. This is consistent with our calculations as illus-

Table 2
List of all the surface reactions used in the model. Rate constant $k = A \times (T)^b \exp(-E/RT)$. A is the pre-exponential factor, b is the temperature exponent and E is the activation energy

No	Surface reactions considered	A (cm-mol-s)	b	E (cal-mol)
1	$CH(S)+H \Rightarrow C(S)+H_2$	1.30×10^{14}	0	7300
2	$C(S)+H_2 \Rightarrow CH(S)+H$	6.50×10^{13}	0	7300
3	$C(S)+H \Rightarrow CH(S)$	1.00×10^{13}	0	0
4	$CH(S) \Rightarrow C(S)+H$	3.30×10^{12}	0	0
5	$C(S)+CH_3 \Rightarrow CCH_3(S)$	5.00×10^{12}	0	0
6	$CCH_3(S) \Rightarrow C(S)+CH_3$	1.00×10^{13}	0	0
7	$C(S)+C_2H_2 \Rightarrow CC_2H_2(S)$	8.00×10^{10}	0	7700
8	$CC_2H_2(S) \Rightarrow C(S)+C_2H_2$	3.20×10^{11}	0	7700
9	$CCH_3(S)+H \Rightarrow CCH_2(S)+H_2$	2.80×10^{7}	0	7700
10	$CCH_2(S)+H_2 \Rightarrow CCH_3(S)+H$	1.40×10^{7}	0	7700
11	$CCH_2(S)+H \Rightarrow CCH_3(S)$	1.00×10^{13}	0	0
12	$CCH_3(S) \Rightarrow CCH_2(S)+H$	3.30×10^{12}	0	0

trated in Fig. 6. The concentrations of CH_3 and C_2H_2 decreased and the CH_4 concentration increased with addition of sulfur as low as 50 ppm. Sulfur aids the formation of CH_4 species by enhancing the recombination of the hydrocarbon radicals.

The sulfur containing radical species, S_2, CS and CS_2, do not increase significantly with increasing concentration of hydrogen disulfide. The steady state computations and mass-spectrometric measurements by Petherbridge [10] for gas phase at 2000 K predicted significant concentrations of CS, CS_2 and S_2 species. The computations using our reaction set for C–H–O–S system at 2000 K reproduced the results in Ref. [10]. The diamond growth kinetics is directly affected by the radical species composition at gas–surface interface at temperatures approximately 1150 K. At this temperature, we observe a decrease in atomic hydrogen concentration with addition of sulfur as shown in Fig. 6. This observation is consistent with Barber and Yarbrough [19] that the gas phase sulfur species lead to faster homogenous recombination kinetics for atomic hydrogen at the substrate and depresses the growth rate. In this regard, the equilibrium calculations cannot predict the kinetic behavior of sulfur containing gas phase due to fast kinetics. A significant difference in the species compositions calculated by equilibrium and steady state calculations was observed in our calculations. The decrease in diamond growth rates under the presence of sulfur should be due to decrease in all the radical species concentrations such as CH_x, C_xH_y, O, OH and H and cannot be attributed to any one of the species. This trend is particularly important with small amount of sulfur in the feed gases, i.e. less than 1000 ppm. At higher concentrations of sulfur in the gas phase, the quality of diamond deposition suffers. In addition, one cannot ignore the surface chemistry of sulfur containing species on the surface for the observed decrease in growth rates.

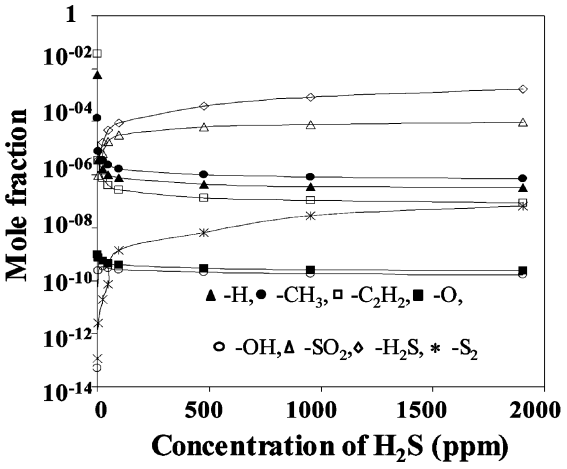

Fig. 3. The changes in resulting gas phase species composition is plotted as a function of increasing sulfur addition to a feed gas phase composition chosen from the non-diamond domain. (Feed gas composition: 10% CH_4, 1% O_2 in H_2). (▲) H, (●) CH_3, (□) C_2H_2, (■) O, (○) OH, (△) SO_2, (◇) H_2S and (*) S_2.

4.4. The effect of Sulfur on the quality of diamond films

Experiments were conducted with increasing sulfur concentration with fixed feed gas compositions to investigate the morphology and quality of the crystals. At lower concentrations of H_2S (0–1000 ppm), well faceted diamond crystals were observed. The morphology of the crystals changed from faceted to more spherical with increasing sulfur concentration in the gas phase as shown in Fig. 8. Micro Raman analysis, shown in Fig.

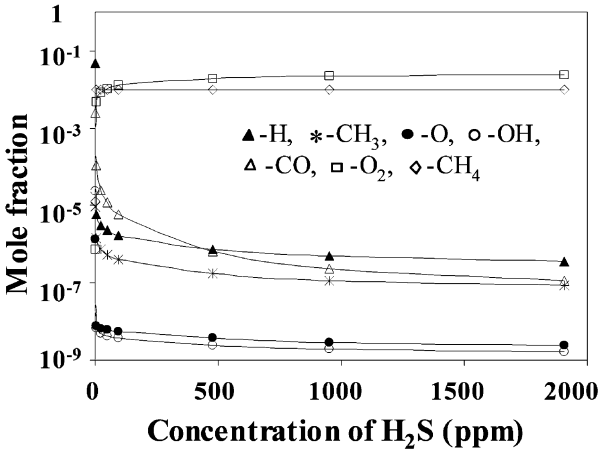

Fig. 4. The species composition is plotted as a function of increasing sulfur addition for a feed gas composition chosen from the no-growth domain. (Feed gas composition: 4% O_2, 1% CH_4 in H_2). (▲) H, (*) CH_3, (●) O, (○) OH, (△) CO, (□) O_2 and (◇) CH_4.

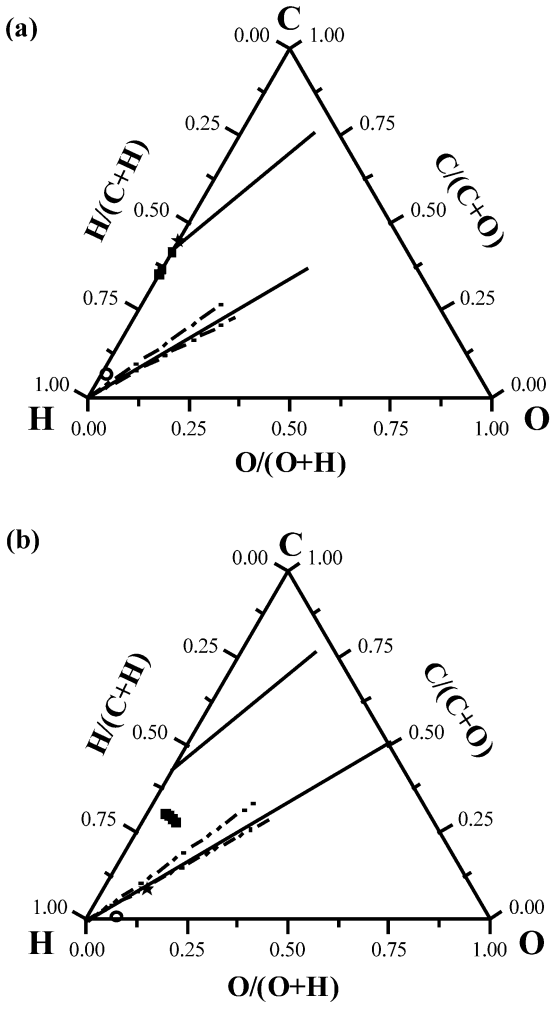

Fig. 5. Illustration of the change in domain with addition of sulfur to feed gas compositions chosen originally from (a) Non-diamond domain feed gases and (b) no-growth domain. (○) represents the feed gas domain while (★) represents the position of this point in the modified radical species diagram. (■) represent the position of the point in the modified diagram with increasing sulfur in the feed gases. The lower part of the Bachmann domain, indicated by dotted lines, is shown for simplicity instead of the lens shaped domain.

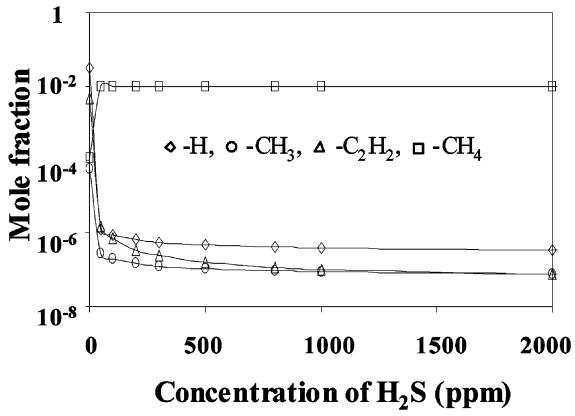

Fig. 6. The resulting concentrations of CH_3, C_2H_2, H and CH_4 with increasing sulfur addition to 1% CH_4 in H_2 feed gases originally from the diamond domain. (◇) H, (○) CH_3, (△) C_2H_2 and (□) CH_4.

8(i), indicates the onset of sp^2 character and a gradual decrease of sp^3 character with increasing sulfur addition. According to the gas phase calculations, the change in the radical species composition beyond 2000 ppm is not significant and cannot explain the drastic decrease in the quality of diamond deposition. At these concentrations of 2000 ppm or higher, the concentrations of sulfur containing species increase and may poison the diamond growth process or promote competing sulfur condensation via direct polymerization reaction.

5. Conclusions

In summary, we have developed a modified C–H–O radical species diagram to predict the diamond deposition in the presence of dopants in the feed gases. The deposition domain on the C–H line has been included for a comprehensive radical diagram. This modified diagram has been used to predict the deposition domain in the presence of sulfur in the gas phase. Addition of sulfur to the no-growth domain feed gases yields diamond growth by binding the oxygen containing species, otherwise dominant without sulfur in the gas phase. The

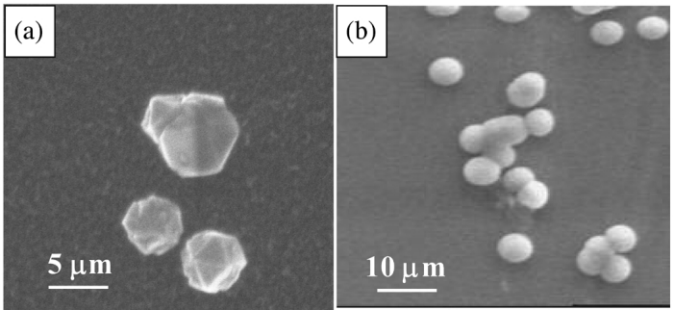

Fig. 7. Scanning electron micrographs of diamond crystals formed with the addition of sulfur to (a) feed gas compositions from no-growth domain and (b) feed gas compositions from non-diamond domain.

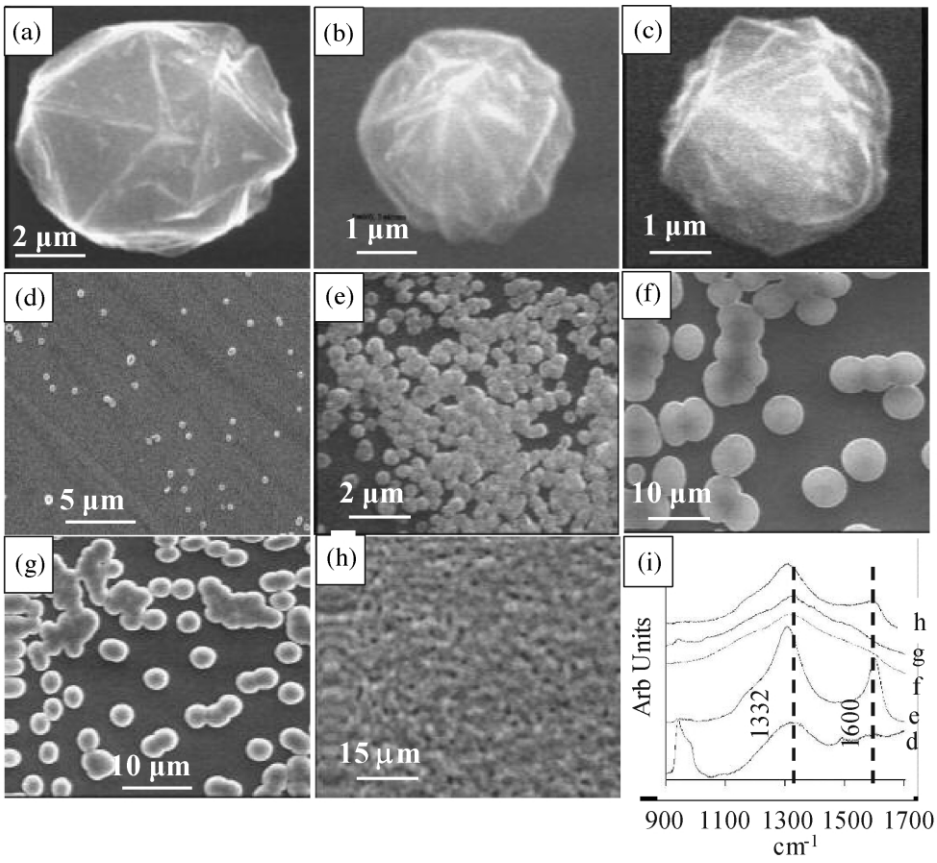

Fig. 8. (a–h) Morphological changes in CVD diamond crystals grown with increased amount of H_2S in the feed gases: (a) 400 ppm, (b) 500 ppm, (c) 740 ppm, (d) 1000 ppm, (e) 2000 ppm, (f) 2500 ppm, (g) 3700 ppm and (h) 7500 ppm. (i) Micro Raman spectrum taken from the crystals shown in (d), (e), (f) and (g). The dashed lines at 1332 cm^{-1} and 1600 cm^{-1} indicate the positions for crystalline diamond and crystalline graphitic, respectively.

oxygen is bound by SO_2 and SO_3. In the case of sulfur addition to non-diamond feed gases, the radical species diagram predicts diamond deposition. This is due to the reduction in carbon super saturation by reduction in the concentrations of C_nH_m species in the gas phase. We attribute the decrease in growth rates due to sulfur addition to diamond domain feed gases to the decrease in concentrations of C_nH_m species. The decrease in quality of diamond grown with increasing sulfur could be due to the surface effects of sulfur at the growth surface. Higher sulfur could lead to the polymerization of sulfur to S_x at the surface, which could impede the diamond growth.

Acknowledgements

Financial support from National Science Foundation (NSF) through CAREER grant (CTS 9876251) is gratefully acknowledged.

References

[1] M.N. Gamo, E. Yasu, C. Xiao, Y. Kikuchi, K. Ushizawa, I. Sakaguchi, T. Suzuki, T. Ando, Diamond Relat. Mater. 9 (2000) 941.

[2] E. Gheeraet, N. Casanova, A. Tajani, A. Deneuville, E. Bustarret, J.A. Garrido, C.E. Nebel, M. Stutzmann, Diamond Relat. Mater. 11 (2002) 289.

[3] J.R. Petherbridge, P.W. May, G.M. Fuge, G.F. Robertson, K.N. Rosser, M.N.R. Ashfold, J. Appl. Phys. 91 (2002) 3605.

[4] S.C. Eaton, A.B. Anderson, J.C. Angus, Y.E. Evstefeeva, Y.V. Pleskov, Electrochem. Solid State Lett. 5 (2002) G65.

[5] J.R. Petherbridge, P.W. May, M.N.R. Ashfold, J. Appl. Phys. 89 (2001) 5219.

[6] S.C. Eaton, M.K. Sunkara, Diamond Relat. Mater. 9 (2000) 1320.

[7] S.C. Eaton, M.K. Sunkara, M. Ueno, K.M. Walsh, Diamond Relat. Mater. 10 (2001) 2212.

[8] D.S. Dandy, Thin Solid films 381 (2001) 1.

[9] H. Sternschulte, M. Schreck, B. Stritzker, Diamond Relat. Mater. 11 (2002) 296.

[10] J.R. Petherbridge, P.W. May, E.J. Crichton, K.N. Rosser, M.N.R. Ashfold, Phys. Chem. Chem. Phys. 4 (2002) 5199.

[11] National Institute of Standards and Technology chemical kinetics database, Standard Reference Database 17, Version 7.0 (web version), http://kinetics.nist.gov.

[12] R.S. Tsang, Ph.D. Thesis, Department of Chemistry, University of Bristol, United Kingdom, 1997.

[13] P.K. Bachmann, D. Leers, H. Lydtin, Diamond Relat. Mater. 1 (1991) 1.

[14] P.K. Bachmann, H. J. Hagemann, H. Late, in: C.H. Carter Jr., G. Gildenblat, S. Nakamura, R. J. Nemanich (Eds.), Diamond SiC and Nitride Wide Bandgap Semiconductors, San Francisco, USA, April 4–8, 1994, Materials Research Society Symposium Proceeding 339 (1994) 267.
[15] N.A. Prijaya, J.C. Angus, P.K. Bachmann, Diamond Relat. Mater. 3/1–2 (1994) 129.
[16] M.R. Zachariah, O.I. Smith, Combust. Flame 69 (1987) 125.
[17] K. Schofield, Combust. Flame 124 (2001) 137.
[18] K. Tsuchiya, K. Kamiya, H. Matsui, Int. J. Chem. Kinet. 29 (1997) 57.
[19] G.D. Barber, W.A. Yarbrough, J. Am. Ceram. Soc. 80 (1997) 1560.